Turkish Journal of Botany
http://journals.tubitak.gov.tr/botany/
Research Article

Turk J Bot
(2019) 43: 358-365

doi:10.3906/bot-1809-27

Wrinkled surface on helical cell wall thickening of vessel elements in flower style

Ming XING, Jian YOU, Xia CHEN*
National and Local United Engineering Laboratory for Chinese Herbal Medicine Breeding and Cultivation, School of Life Sciences, Jilin University, Changchun, Jilin Province, P.R. China

Received: 17.09.2018 • **Accepted/Published Online:** 24.02.2019 • **Final Version:** 06.05.2019

Abstract: In the present study, wrinkled surfaces were discovered on the cell wall thickenings of helical vessels in the lilac style for the first time. The structure of the wrinkles was formed by cellulose microfibrils, with convex ridges composed of crystalline cellulose and concave grooves composed of amorphous cellulose. The cellulose microfibrils were oriented with the helical cell wall thickenings. The wrinkle morphology was due to the aligned crystalline region of the microfibrils. The wrinkle structure in the flower style might be related to the faster growth rate of style tissues during helix cell wall thickening development. Discovery of the wrinkled surface could help with the study of the developmental mechanism of helical vessel cells.

Key words: Cellulose, helix, vessel, style, thickening

1. Introduction

In the present study, we discovered a unique wrinkle surface morphology on helical cell wall thickenings. Cell wall thickening is the most important character of botanical vessel cells. Cell wall thickening in different tissues shows varied surface morphology, such as parallel cellulose fibrils in *Zinnia elegans* leaves (Lacayo et al., 2010) and cellulose lamellas in wheat straw stems (Yu et al., 2005). However, there are still undiscovered surface morphologies of cell wall thickenings. The various morphologies are caused by different cellulose synthases' release, arrangement, movement, direction, and lifetime (Wightman and Turner, 2008). Additionally, different types of cellulose synthases can cause different cellulose microfibril structures (Kumar et al., 2018).

Wall thickening is a specific cell wall that is widely present in tracheary elements. The cell wall outside the plant cell membrane usually includes two types: the primary cell wall and the secondary cell wall. The primary cell wall is a thin layer, whereas the secondary cell wall inside the primary cell wall provides more mechanical support for cells. Tracheary elements exist in vascular plants. Tracheary elements lack contents at maturation and transport water for tissues as hollow pipes, utilizing wall thickenings as skeletons to hold the outside primary cell wall (Rudall, 2007).

Wall thickenings contain cellulose, hemicellulose, pectin, and lignin. Cellulose is the skeleton and the other components resemble concrete which enwraps the cellulose. Wall thickenings increase the surface area and promote water conduction (Monniaux and Hay, 2016). Pectin is hydrophilic (Bagniewska-Zadworna et al., 2014). The cellulose microfibrils in the lignified secondary thickening are typically oriented in a preferred direction, causing cell walls to be mechanically anisotropic (Nelson et al., 2012).

Helical wall thickenings are most commonly found in vessel elements (a type of tracheary element) and can mechanically stabilize the tissue, allowing the maximal uptake of water (Leroux et al., 2011). The organization of cellulose in helical wall thickenings is due to the movement of cellulose synthesis complexes (CSCs). In the plasma, CSCs are transported by actin and secreted by the Golgi apparatus (Derbyshire et al., 2015; Watanabe et al., 2015). When CSCs reach the right position determined by microtubules (Wightman and Turner, 2008), they fuse outside the membrane and move to produce cellulose along the helical direction of the microtubules (Roberts et al., 2004; Vukašinović et al., 2017). Wall thickenings in different types of tissues show various patterns of cellulose microfibrils (Yu et al., 2005; Lacayo et al., 2010), which may be related to the functions of the different tissues.

In the present study, we researched the helical vessel elements in the lilac (*Syringa oblata* Lindl.) style. The style is a specialized tissue that interacts with the pollen tube and facilitates its access to the female gametophyte

* Correspondence: chenxiajlu@163.com

in angiosperms (Williams et al., 2010). It contains the stigma and transmitting tissues. During angiosperm reproduction, pollen grains that are germinated on the stigma surface form a pollen tube that grows through the transmitting tissues to the ovule micropyle (Palanivelu et al., 2003). The style is a fragile and short-lived tissue (Gotelli et al., 2017) which grows and wilts fast, within no longer than 2 weeks. The helical thickening vessel is the only tissue to provide water for the stigma, transmitting tissue, female gametophyte, and pollen tube. Additionally, helical thickening vessels are the only mechanical tissue in the lilac style.

We discovered a unique wrinkled surface morphology on the helical cell wall thickenings of vessels in the short-lived lilac style. We studied the structures of the wrinkles and attempted to explain the developmental mechanism of the wrinkles. The wrinkles were composed of orderly organized crystalline and amorphous cellulose. The style morphology is different from the wall thickenings in other tissues (e.g., leaves, stems, and pollen). The special wrinkle structures were caused by regularly arranged cellulose microfibrils. The results might relate to the process of cellulose production in helical thickening vessels. The strange structure of the helical vessel in the lilac style might also be related to the fast growth of the style.

2. Materials and methods

2.1. Materials

The pistil of lilac (*Syringa oblata*) was treated thoroughly using a combination of methods to remove pectin, lignin, and other noncellulosic substances completely. The details of the purification method have been presented previously (Kataoka and Kondo, 1998; Liu et al., 2005; Yu et al., 2005). To describe it here shortly, each sample was immersed in chloroform–ethanol (1:1, v/v) overnight and then transferred into acetone to replace the residual chloroform and ethanol. After the acetone was replaced by distilled water, the sample was subjected to water extraction at 90 °C for 6 h. The sample was then treated with 0.5% ammonium oxalate at 70 °C for another 6 h. It was then extracted twice with 0.3% dodecyl sulfate for 12 h and with an aqueous solution of 50% urea for another 12 h at room temperature. The sample was subjected to bleaching at 80 °C for 4 h in a 0.3% sodium chlorite ($NaClO_2$) aqueous solution buffered with acetic acid at pH 4.9. The helical vessels were isolated from the sample with needles under a microscope. The dispersed vessel was then transferred into tert-butyl alcohol and freeze-dried on a fresh cleaved silicon surface for AFM and SEM analysis. All treatments described above were achieved by gently shaking. The primary cell wall was digested with 2% snail enzyme in 0.1M phosphate buffered saline (PBS) (pH 7.2) at 30 °C for 1 h. The reagents were all purchased from Sigma-Aldrich (St. Louis, MO, USA).

2.2. Scanning electron microscopy (SEM) analysis

SEM analysis was performed with a Quanta 200 SEM (FEI, Hillsboro, OR, USA), operated at 15 kV. The freeze-dried samples were coated with gold using an IB-3 incoater (Eiko, Ibaraki, Japan).

2.3. Atomic force microscope (AFM) analysis

Tapping-mode AFM images were obtained by using a NanoScope III Multimode AFM (Vecco/Digital Instruments, Santa Barbara, CA, USA). Both topographic and phase images were recorded simultaneously. Silicon cantilever tips with a resonance frequency of approximately 300 kHz and a spring constant of about 32 N/m were used.

2.4. Laser confocal microscope

The method visualizing orientation of cellulose is based on the fluorescence dichroism of Congo red (Wood, 1980; Verbelen and Kerstens, 2000; Kerstens and Verbelen, 2003). Cellulose microfibrils in helical cell wall thickenings were stained with a 1% aqueous solution of Congo Red (Sigma-Aldrich, St. Louis, MO, USA) at 37 °C for 30 min. The dyed samples were rinsed with water and studied with a laser confocal microscope (Olympus FV300, Tokyo, Japan) equipped with a coaxial rotating table. For all observations, the 514 nm line of the laser source was used. A polarizing filter was inserted into the exciting beam such that the vector of the exciting beam was vertical on the microscope monitor.

2.5. Fourier transform infrared spectroscopy (FTIR) analysis

The samples (1 mg) and potassium bromide (100 mg) were mixed using a mortar and pestle, and thereafter pressed into a transparent disk. The disk was analyzed with a Nicolet 5700 FTIR spectrometer (Thermo Fisher Scientific, Madison, WI, USA) in the absorbance mode with a resolution of 1 cm^{-1} in the range 4000–400 cm^{-1}.

3. Results

The surface morphology of cell wall thickenings is caused by the arrangement of the cellulose. Cell wall thickening usually includes cellulose and noncellulosic components. Cellulose is the skeleton of the cell wall thickening. Lignin, hemicellulose, and pectin enclose the cellulose skeleton and interfere with examination of the surface. Thus, to identify the wrinkled surface on the cell wall thickening, we removed the noncellulosic components. FTIR was used to examine the elimination effect (Figure 1). FTIR showed that there were no other cell wall ingredients except for cellulose.

The characteristic bands of lignin at approximately 1500 cm^{-1} (K.V. Sarkanen, 1971) and hemicellulose at 1600 cm^{-1} (Horikawa and Sugiyama, 2008; Abdul Khalil et al., 2010) were not found using FTIR. The peaks assigned to the esterified carboxyl groups in pectin at 1734 cm^{-1} (Ninan et al., 2013) were also not observed. Therefore, the

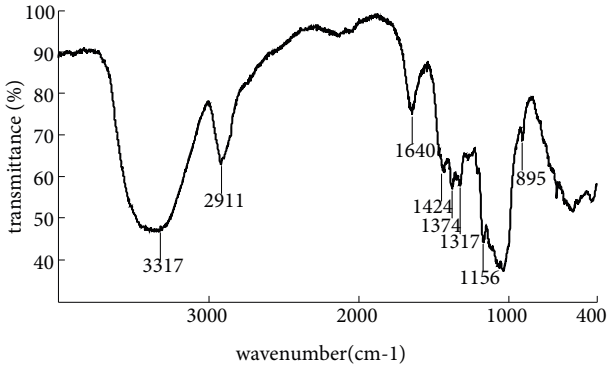

Figure 1. FTIR spectra of the cell wall thickenings treated to remove noncellulosic substances. FTIR was used to examine the components of the sample. Only the characteristic bands of cellulose were found. There were no characteristic bands of noncellulosic components, such as pectin, hemicellulose, and lignin. Thus, the sample contained cellulose without noncellulosic components. The wrinkle structures were formed by cellulose.

noncellulosic components had been removed properly. The generally accepted characteristic FTIR bands for cellulose were monitored as follows: 3317 cm^{-1} for intrachain hydrogen-bond bonds, 1424 cm^{-1} for CH_2 scissoring vibrations, 1374 cm^{-1} for C-H skeletal bending of CH_3, 1317 cm^{-1} for the CH_2 wagging observed in crystalline cellulose, and 1156 and 895 cm^{-1} for the C–O–C movement of the β glycoside linkage (Mary and Robert, 1964; Kacurakova et al., 2000; Marechal and Chanzy, 2000; Carballo-Meilan et al., 2014). The wrinkle structure was completely formed of cellulose.

The wall thickening of vessels in the lilac style formed a helix (Figure 2a). The vessels were all dead cells and transported water for the pistil and pollen tube. The diameters of the vessels in the lilac style were 5–7 μm. The dead vessels included the primary cell wall on the outside and cell wall thickenings under the primary cell wall. The width of the helical wall thickenings was between 1200 and 1500 nm.

The wrinkled surface that was found existed on the cell wall thickening. When noncellulosic components have been removed properly, the wrinkled surface can be observed by AFM and SEM (Figures 2b, 3a, and 3b). The wrinkles can be found on the surface of the cell wall thickening. The primary cell wall showed a smooth surface without the wrinkled surface. More than 20 samples were tested, and the wrinkled surface of the cell wall thickening were found in each sample.

To see the wrinkled surface of the secondary wall thickening more clearly, we used snail enzyme to hydrolyze the cell wall. Snail enzyme can nonselectively damage cellulose including the primary cell wall and wall thickenings. The primary cell wall was more easily hydrolyzed (Figure 3a). When abundant primary cell walls were absent, the spatial helix was hard to maintain (Figure 4a). Although hydrolysis on the surface of the secondary cell wall thickening was impossible to avoid, wrinkles on the wall thickening with partial hydrolysis were illuminated more clearly (Figures 3b and 4b).

The wrinkled surface was composed of orderly organized cellulose. The width of the wrinkles was measured after enzyme hydrolysis. The width was between 172 nm and 244 nm, with a mean of 207 nm (Figure 4b). The width corresponded to the crystals of cellulose microfibrils in previous studies (Nishiyama et al., 2003; Alemdar and Sain, 2008; Elazzouzi-Hafraoui et al., 2008; Habibi et al., 2010; Lavoine et al., 2012; Nishiyama et al., 2012).

To determine the arrangement orientation of cellulose in the wrinkled surface, the molecular orientations were tested using Congo Red. The molecular orientation of cellulose is the growth orientation of cellulose that is produced by cellulose synthase complexes. The fluorophore Congo Red typically binds to the β 1-4 glucans of cellulose (Wood, 1980). When bound to cellulose, the average dipole moment of Congo Red can lie parallel to the orientation of the cellulose microfibril (Verbelen and Kerstens, 2000). The fluorescence of Congo Red is at a maximum when the vector of the exciting laser of a confocal microscope is parallel to the microfibril orientation, and it is at a minimum when the vector of the laser is perpendicular to the microfibrils (Kerstens and Verbelen, 2003). In Figure 5, the orientation of the polarization vector is indicated by arrows. Fluorescence was false color-coded to show fluorescence intensity, where red indicated the highest fluorescence intensity and blue showed the lowest. The vessels had a cellulose orientation parallel to the tangential direction of the spiral line. The cellulose in the wrinkled surface was perpendicular to the grooves in the wrinkles.

The arrangement of cellulose microfibrils in the wrinkle structure was tested by AFM. The wrinkled surface formed a ridge–groove structure on the cell wall thickenings (Figures 3b and 4b). A 3D representation showed concave grooves between convex ridges (Figure 4c). The direction of the cellulose microfibril was perpendicular to the grooves and ridges. Conformation of cellulose in the ridges was apparent in the phase image (Figure 4d). In this image, lighter regions corresponded to crystalline regions with higher stiffness; these regions were associated with aggregative cellulose (Zimmermann et al., 2006). The crystalline cellulose all aggregated in the convex ridge. The darker areas in the image were composed of amorphous regions, which had lower density and more disordered cellulose. The groove was composed of amorphous cellulose with an average width of approximately 10 nm. The ridge mainly comprised aligned crystalline regions.

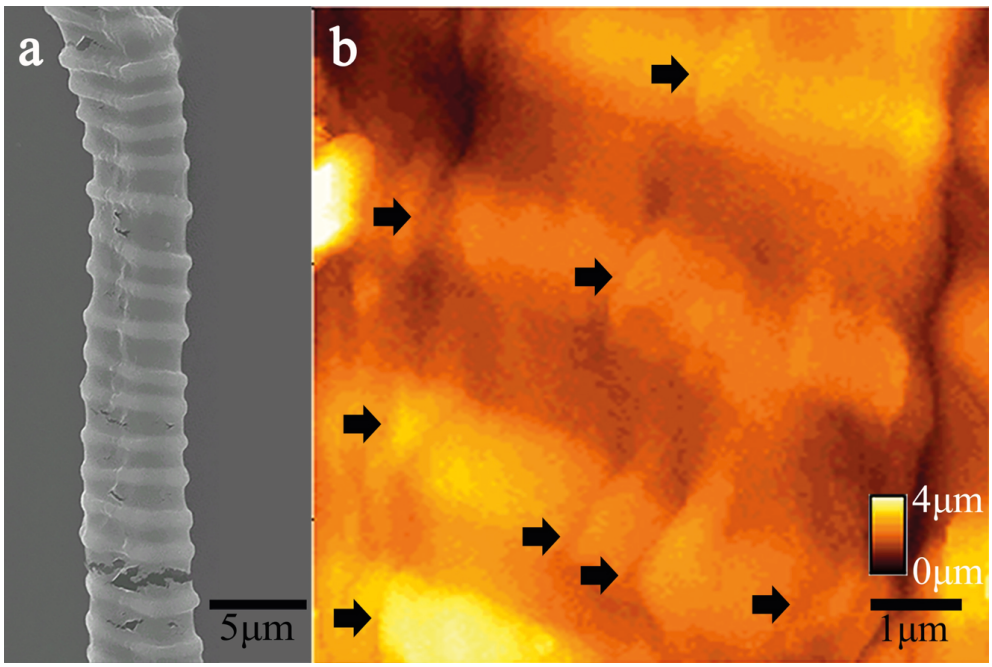

Figure 2. The wrinkled surface of helical cell wall thickening with primary cell wall. Before the snail enzyme digestion, both primary cell wall and secondary cell wall thickenings were integrated. (a): the samples were tested with SEM. (b): the samples were observed with AFM. The wrinkles (black arrow) existed on the cell wall thickenings. The primary cell wall showed a smooth surface without wrinkles. Because the primary cell wall was above the secondary thickenings, the wrinkles of the cell wall thickenings observed with AFM were indistinct.

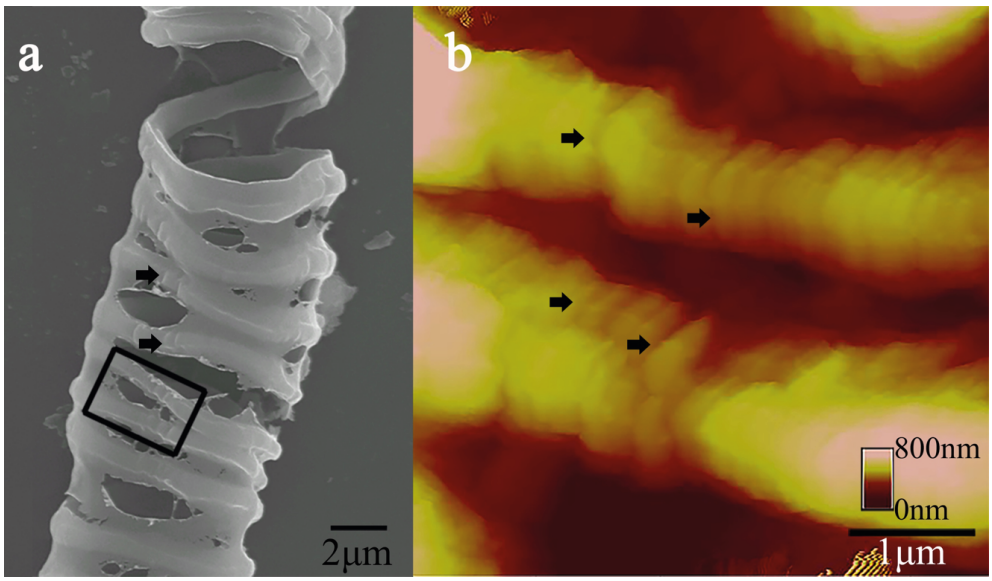

Figure 3. The wrinkled surface of helical cell wall thickening with partially digested primary cell wall. The samples had been treated with snail enzyme. Part of primary cell wall had been digested. (a): the samples were tested with SEM. (b): the samples were observed with AFM. Compared with the samples before enzyme digestion, the wrinkles (black arrow) on thickenings were illuminated more clearly. It was proved that the wrinkles existed on the thickenings, not on the primary cell wall.

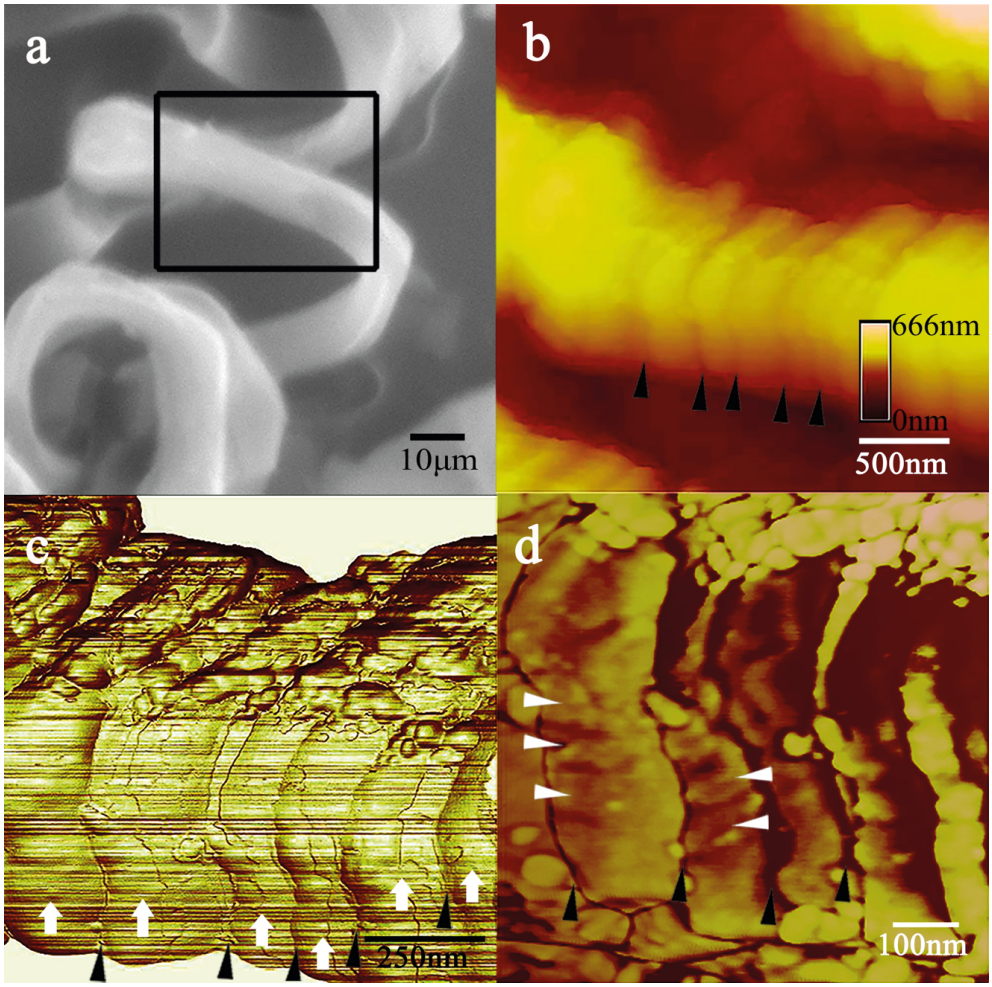

Figure 4. The wrinkled surface of helical cell wall thickening without the primary cell wall. Most of the primary cell wall of the sample had been digested with snail enzyme. (a): the samples were tested with SEM. Without the primary cell wall between the helical thickenings, the spatial helix was hard to maintain. The region in the black frame was tested with AFM. (b): the sample was observed with AFM. The wrinkles on the cell wall thickening are indicated with black triangles. (c): a 3D rendering of the wrinkles on the thickened cellulose surface. The wrinkles consisted of a convex ridge region (white arrow) and concave groove region (black triangle). The direction of the spiral line was perpendicular to the grooves and ridges. (d) The local magnified phase image of the wrinkle structures. There was crystalline cellulose (lighter areas) and amorphous cellulose (darker areas). The crystalline cellulose (white triangle) was approximately 207 nm in average length and 66 nm in average width. The amorphous cellulose in the groove of the wrinkle structures (black triangle) was about 10nm in width.

In the ridge, the adjacent crystalline regions of microfibrils were arranged in sequence and were parallel to each other. The crystalline cellulose was approximately 207 nm in average length and 66 nm in average width.

4. Discussion

Wrinkles on the surface of cell wall thickenings are a special topology of cellulose crystal. The crystalline microfibrils in the lilac style were arranged more regularly than those in the common secondary cell wall (Yu et al., 2005; Lacayo et al., 2010). The convex ridges of the wrinkles were composed of orderly crystalline cellulose. The grooves were amorphous cellulose and the molecular orientation of the cellulose was consistent with the direction of helix wall thickenings. Thus, we have attempted to determine and discuss how the wrinkles developed in the lilac style.

Previous studies have proven that the construction of secondary cell walls is different from the mechanism observed in primary cell walls (Lei et al., 2012). Cellulose is a major component of plant cell walls, together with

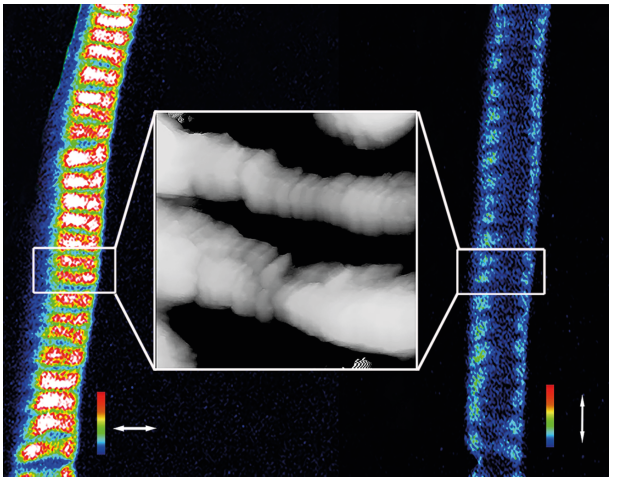

Figure 5. The orientation of cellulose microfibril in the wrinkles on helical cell wall thickenings. The confocal micrographs showed differences of fluorescence intensity of cellulose after Congo Red staining with different directions of polarization vector. Fluorescence intensity was coded with false color. Red showed the highest fluorescence intensity and blue showed the lowest. The orientation of polarization vector is indicated by the white arrows. The fluorescence of cellulose microfibrils on the left side was at a maximum when the polarization was parallel to the spiral line. The lowest fluorescence intensity was on the right side when the polarization vector was perpendicular to the spiral line. The middle picture showed the direction of wrinkles of helical thickenings in the black frame. The fluorescence showed that cellulose microfibrils in the wrinkles were parallel with the tangential direction of the spiral line.

hemicellulose and lignin. In secondary cell walls, several cellulose molecules are brought together into larger units known as microfibrils (Lavoine et al., 2012). These packed microfibrils are strings of crystalline cellulose that are connected along their length by amorphous cellulose (Azizi Samir et al., 2005). For primary cell wall synthesis, microtubules mark the site for the delivery of CSCs to the plasma membrane (Crowell et al., 2009; Gutierrez et al., 2009).

Previous studies have found that actin microfilaments are correlated with cellulose deposition during the synthesis of secondary walls (Seagull, 1990; Mutwil et al., 2008; Wightman and Turner, 2008). The arrangement of cellulose in helical vessels is predetermined by the movement of the Golgi apparatus (Habibi et al., 2010; Lei et al., 2012). The Golgi apparatus transports CSCs along thick actin cables in xylem vessels and remains at a particular position for 2–4 s to secrete CSCs to the membrane (Gardiner et al., 2003; Wightman and Turner, 2008; Wightman and Turner, 2010). The end points of deposition are determined by the crossing points of actin fibers and cable, where there are several linear regions along the long axis of the vessel (actin cables) (Gardiner et al., 2003; Wightman and Turner, 2008; Carpita, 2012; Worden et al., 2012). CSCs produce microfibrils along the short axis (actin fibers) (Wightman and Turner, 2010).

Therefore, it was hypothesized that there was a great chance that the microfibril ends (the crossing points) might be aligned with the actin cables, which were along the long axis of the vessel cells. Because microfibrils have periodically arranged crystalline regions and amorphous regions, the aligned microfibrils may form regular structures. However, there have been no detailed studies of microfibril structures to test this hypothesis to date.

The wrinkle structure reported in the present study could be the evidence to support this hypothesis. The convex ridges were aligned crystalline regions of cellulose microfibrils, because the aligned microfibrils had an approximate length of the crystalline regions (207 nm on average) and periodic disordered regions (10 nm on average). Therefore, the aligned microfibrils must have been the aligned starting points. The starting points were thought to be where CSCs began to deposit cellulose and form microfibrils (Wightman and Turner, 2010). Thus, CSCs should be secreted at several aligned positions. The initial microfibrils should be near these positions. Because the Golgi apparatus transported and released CSCs along the long axis of vessel cells, the starting points of the microfibrils were aligned to the long axis (Gardiner et al., 2003; Wightman and Turner, 2010; Carpita, 2012; Worden et al., 2012). Additionally, the speed of CSCs was almost the same (Paredez et al., 2006; Guerriero et al., 2010; Lei et al., 2012), and the lengths of the crystalline regions in one plant tended to be equal (Habibi et al., 2010). Therefore, the aligned release and movement of CSCs caused the crystalline regions to be aligned with each other and form regular ridge–groove structures (i.e., wrinkles).

The wrinkles in the lilac style might be a special example of helical vessel development because the lilac style grew and wilted more quickly than other tissues, such as stems or leaves. Therefore, the helical vessel developed and formed faster than that of helical vessels in other tissues. In the faster developing rates, the Golgi apparatus might transport and secrete CSCs more intensely. The helical thickenings had more obverse aligned microfibrils than other tissues.

Consequently, a wrinkled surface on secondary cell walls was discovered for the first time and investigated in helical vessels of the lilac style. The wrinkle morphology was due to the aligned crystalline region of cellulose microfibrils. The regular structure might be caused by regular release of CSCs.

Acknowledgments

The paper was supported by the fund of the Laboratory and Equipment Management Department of Jilin University and the open research foundation of Academy of Science of Changbai Mountain in China (201701).

References

Abdul Khalil HPS, Yusra AFI, Bhat AH, Jawaid M (2010). Cell wall ultrastructure, anatomy, lignin distribution, and chemical composition of Malaysian cultivated kenaf fiber. Industrial Crops and Products 31(1): 113-121.

Alemdar A, Sain M (2008). Isolation and characterization of nanofibers from agricultural residues: wheat straw and soy hulls. Bioresource Technology 99(6): 1664-1671.

Azizi Samir MAS, Alloin F, Dufresne A (2005). Review of recent research into cellulosic whiskers, their properties and their application in nanocomposite field. Biomacromolecules 6(2): 612-626.

Bagniewska-Zadworna A, Arasimowicz-Jelonek M, Smoliński DJ, Stelmasik A (2014). New insights into pioneer root xylem development: evidence obtained from *Populus trichocarpa* plants grown under field conditions. Annals of Botany 113(7): 1235-1247.

Carballo-Meilan A, Goodman AM, Baron MG, Gonzalez-Rodriguez J (2014). A specific case in the classification of woods by FTIR and chemometric: discrimination of Fagales from Malpighiales. Cellulose 21(1): 261-273.

Carpita NC (2012). Progress in the biological synthesis of the plant cell wall: new ideas for improving biomass for bioenergy. Current Opinion in Biotechnology 23(3): 330-337.

Crowell EF, Bischoff V, Desprez T, Rolland A, Stierhof YD et al. (2009). Pausing of Golgi bodies on microtubules regulates secretion of cellulose synthase complexes in *Arabidopsis*. The Plant Cell 21(4): 1141-1154.

Derbyshire P, Ménard D, Green P, Saalbach G, Buschmann H et al. (2015). Proteomic analysis of microtubule interacting proteins over the course of xylem tracheary element formation in *Arabidopsis*. The Plant Cell 27(10): 2709-2726.

Elazzouzi-Hafraoui S, Nishiyama Y, Putaux JL, Heux L, Dubreuil F et al. (2008). The shape and size distribution of crystalline nanoparticles prepared by acid hydrolysis of native cellulose. Biomacromolecules 9(1): 57-65.

Gardiner JC, Taylor NG, Turner SR (2003). Control of cellulose synthase complex localization in developing xylem. The Plant Cell 15(8): 1740-1748.

Gotelli MM, Lattar EC, Zini LM, Galati BG (2017). Style morphology and pollen tube pathway. Plant Reproduction 30(4): 155-170.

Guerriero G, Fugelstad J, Bulone V (2010). What do we really know about cellulose biosynthesis in higher plants? Journal of Integrative Plant Biology 52(2): 161-175.

Gutierrez R, Lindeboom JJ, Paredez AR, Emons AMC, Ehrhardt DW (2009). *Arabidopsis* cortical microtubules position cellulose synthase delivery to the plasma membrane and interact with cellulose synthase trafficking compartments. Nature Cell Biology 11(7): 797-806.

Habibi Y, Lucia LA, Rojas OJ (2010). Cellulose nanocrystals: chemistry, self-assembly, and applications. Chemical Reviews 110(6): 3479-3500.

Horikawa Y, Sugiyama J (2008). Accessibility and size of *Valonia* cellulose microfibril studied by combined deuteration/rehydrogenation and FTIR technique. Cellulose 15(3): 419-424.

K.V. Sarkanen CHL (1971). Lignins: Occurrence, Formation, Structure and Reactions. New York, NY, USA: Wiley Interscience.

Kacurakova M, Capek P, Sasinkov V, Wellner N, Ebringerov A (2000). FT-IR study of plant cell wall model compounds: pectic polysaccharides and hemicelluloses. Carbohydrate Polymers 43(2): 195-203.

Kataoka Y, Kondo T (1998). FT-IR microscopic analysis of changing cellulose crystalline structure during wood cell wall formation. Macromolecules 31(3): 760-764.

Kerstens S, Verbelen J-P (2003). Cellulose orientation at the surface of the *Arabidopsis* seedling: implications for the biomechanics in plant development. Journal of Structural Biology 144(3): 262-270.

Kumar M, Mishra L, Carr P, Pilling M, Gardner P et al. (2018). Exploiting CELLULOSE SYNTHASE (CESA) class specificity to probe cellulose microfibril biosynthesis. Plant Physiology 177(1): 151-167.

Lacayo CI, Malkin AJ, Holman HY, Chen L, Ding SY et al. (2010). Imaging cell wall architecture in single *Zinnia elegans* tracheary elements. Plant Physiology 154(1): 121-133.

Lavoine N, Desloges I, Dufresne A, Bras J (2012). Microfibrillated cellulose – Its barrier properties and applications in cellulosic materials: a review. Carbohydrate Polymers 90(2): 735-764.

Lei L, Li S, Gu Y (2012). Cellulose synthase complexes: structure and regulation. Frontiers in Plant Science 3: 1-6. doi:10.3389/fpls.2012.00075.

Leroux O, Bagniewska-Zadworna A, Rambe SK, Knox JP, Marcus SE et al. (2011). Non-lignified helical cell wall thickenings in root cortical cells of *Aspleniaceae* (Polypodiales): histology and taxonomical significance. Annals of Botany 107(2): 195-207.

Liu R, Yu H, Huang Y (2005). Structure and morphology of cellulose in wheat straw. Cellulose 12(1): 25-34.

Marechal Y, Chanzy H (2000). The hydrogen bond network in I-beta cellulose as observed by infrared spectrometry. Journal of Molecular Structure 523(1): 183-196.

Mary LN, Robert TOC (1964). Relation of certain infrared bands to cellulose crystallinity and crystal lattice type. Part II. A new infrared ratio for estimation of crystallinity in celluloses I and II. Journal of Applied Polymer Science 8(3): 1325-1341.

Monniaux M, Hay A (2016). Cells, walls, and endless forms. Current Opinion in Plant Biology 34: 114-121.

Mutwil M, Debolt S, Persson S (2008). Cellulose synthesis: a complex complex. Current Opinion in Plant Biology 11(3): 252-257.

Nelson MR, Band LR, Dyson RJ, Lessinnes T, Wells DM et al. (2012). A biomechanical model of anther opening reveals the roles of dehydration and secondary thickening. New Phytologist 196(4): 1030-1037.

Ninan N, Muthiah M, Park I-K, Elain A, Thomas S et al. (2013). Pectin/carboxymethyl cellulose/microfibrillated cellulose composite scaffolds for tissue engineering. Carbohydrate Polymers 98(1): 877-885.

Nishiyama Y, Johnson G, French A (2012). Diffraction from nonperiodic models of cellulose crystals. Cellulose 19(2): 319-336.

Nishiyama Y, Kim UJ, Kim DY, Katsumata KS, May RP et al. (2003). Periodic disorder along ramie cellulose microfibrils. Biomacromolecules 4(4): 1013-1017.

Palanivelu R, Brass L, Edlund AF, Preuss D (2003). Pollen tube growth and guidance is regulated by POP2, an *Arabidopsis* gene that controls GABA levels. Cell 114(1): 47-59.

Paredez AR, Somerville CR, Ehrhardt DW (2006). Visualization of cellulose synthase demonstrates functional association with microtubules. Science 312(5779): 1491-1495.

Roberts AW, Frost AO, Roberts EM, Haigler CH (2004). Roles of microtubules and cellulose microfibril assembly in the localization of secondary-cell-wall deposition in developing tracheary elements. Protoplasma 224(3-4): 217-229.

Rudall PJ (2007). Anatomy of Flowering Plants. New York, NY, USA: Cambridge University Press.

Seagull RW (1990). The effects of microtubule and microfilament disrupting agents on cytoskeletal arrays and wall deposition in developing cotton fibers. Protoplasma 159(1): 44-59.

Verbelen, Kerstens (2000). Polarization confocal microscopy and Congo Red fluorescence: a simple and rapid method to determine the mean cellulose fibril orientation in plants. Journal of Microscopy 198(2): 101-107.

Vukašinović N, Oda Y, Pejchar P, Synek L, Pečenková T et al. (2017). Microtubule-dependent targeting of the exocyst complex is necessary for xylem development in *Arabidopsis*. New Phytologist 213(3): 1052-1067.

Watanabe Y, Meents MJ, McDonnell LM, Barkwill S, Sampathkumar A et al. (2015). Visualization of cellulose synthases in *Arabidopsis* secondary cell walls. Science 350(6257): 198-203.

Wightman R, Turner S (2010). Trafficking of the cellulose synthase complex in developing xylem vessels. Biochemical Society Transactions 38(3): 755-760.

Wightman R, Turner SR (2008). The roles of the cytoskeleton during cellulose deposition at the secondary cell wall. The Plant Journal 54(5): 794-805.

Williams JH, McNeilage RT, Lettre MT, Taylor ML (2010). Pollen tube growth and the pollen-tube pathway of *Nymphaea odorata* (Nymphaeaceae). Botanical Journal of The Linnean Society 162(4): 581-593.

Wood PJ (1980). Specificity in the interaction of direct dyes with polysaccharides. Carbohydrate Research 85(2): 271-287.

Worden N, Park E, Drakakaki G (2012). Trans-Golgi network-an intersection of trafficking cell wall components. Journal of Integrative Plant Biology 54(11): 875-886.

Yu H, Liu RG, Shen DW, Jiang Y, Huang Y (2005). Study on morphology and orientation of cellulose in the vascular bundle of wheat straw. Polymer 46(15): 5689-5694.

Zimmermann T, Thommen V, Reimann P, Hug HJ (2006). Ultrastructural appearance of embedded and polished wood cell walls as revealed by Atomic Force Microscopy. Journal of Structural Biology 156(2): 363-369.